Room-temperature intrinsic ferromagnetism in epitaxial CrTe2 ultrathin films

Xiaoqian Zhang,[1,2#] Qiangsheng Lu,[2#] Wenqing Liu,[1,3#] Wei Niu,[4] Jiabao Sun,[3] Jacob Cook,[2] Mitchel Vaninger,[2] Paul. F. Miceli,[2] David J. Singh,[2,5] Shang-Wei Lian,[6] Tay-Rong Chang,[6,7] Liang He,[1*] Yongbing Xu,[1,8*] Guang Bian[2*]

[1]Jiangsu Provincial Key Laboratory of Advanced Photonic and Electronic Materials, Collaborative Innovation Center of Advanced Microstructures, School of Electronic Science and Engineering, Nanjing University, Nanjing 210093, China

[2]Department of Physics and Astronomy, University of Missouri, Columbia, Missouri 65211, USA

[3]Department of Electronic Engineering, Royal Holloway University of London, Egham, Surrey TW20 0EX, UK

[4]New Energy Technology Engineering Laboratory of Jiangsu Provence & School of Science, Nanjing University of Posts and Telecommunications, Nanjing 210023, China

[5]Department of Chemistry, University of Missouri, Columbia, Missouri 65211, USA

[6]Department of Physics, National Cheng Kung University Tainan 701, Taiwan

[7]Center for Quantum Frontiers of Research and Technology (QFort), Tainan 701, Taiwan

[8]York-Nanjing Joint Centre (YNJC) for spintronics and nano engineering, Department of Electronic Engineering, The University of York, YO10 3DD, United Kingdom

[#]These authors contribute equally to this work.

*Correspondence and requests for materials should be addressed to G.B. (E-mail: biang@missouri.edu), Y.X. (ybxu@nju.edu.cn), L.H. (heliang@nju.edu.cn)

Abstract

Uncovering the intrinsic two-dimensional (2D) ferromagnetism in layered compounds and exfoliated thin films provides extraordinary functionalities for device applications. However, due to the reduced dimensionality, 2D magnets usually exhibit weak magnetic ordering compared to conventional bulk magnets. This is seen in the lower Curie temperatures (T_c) typically found in 2D materials. Here, we report a new approach to realize 2D magnets by using molecular beam epitaxy (MBE). The epitaxial $CrTe_2$ films show remarkable robustness and strength of magnetic order. We discover that the T_c of 7-monolayer $CrTe_2$ (~ 4 nm) is 254 K and the atomic magnetic moment is ~3 μ_B/atom, according to XMCD and SQUID measurements. Both Curie temperature and atomic magnetic moments are highest among 2D magnetic materials. In addition, the thin films fabricated through MBE possess atomically uniform surfaces, enabling a direct photoemission characterization. Our ARPES measurements show unambiguously the majority and minority electronic states of magnetic nanofilms for the first time, revealing the spin polarized electronic structure of the 2D magnet. Taking the results collectively, our work demonstrates a practical methodology for realizing robust 2D ferromagnetic states in MBE thin films and provides ideal materials infrastructure for nano-spintronics.

Two-dimensional (2D) layered ferromagnetic materials have attracted much interest recently since the discovery of intrinsic 2D ferromagnetism in atomically thin layers[1-6]. Shortly afterwards, enormous research efforts have been placed on enhancing ferromagnetic order in intrinsic 2D magnets. 2D magnetic materials with a robust magnetic ordering are critically important for nano-spintronics applications and to provide platforms for developing scientific understanding of 2D magnetism and phenomena such as topological defects in 2D. To enhance the robustness of 2D ferromagnets, three routes have been proposed and tested. The first route is doping a ferromagnetic host with specific elements, resulting in a limited increase of Curie temperature (T_c) but unavoidable clusters and/or disorder from dopants[7,8]. The second route is constructing heterostructures with ferromagnetic (or ferrimagnetic) metals (or insulators), in which the ferromagnetic order can be enhanced by proximity effects[9-12]. For instance, the $(Fe_3GeTe_2/MnTe)_3$ superlattices possess a larger coercive field as a result of proximity effect[8]. However, the penetration depth of proximity effect is usually very small (< 5nm), hindering an effective manipulation of magnetic order. The third method is controlling magnetic ordering by ionic liquid gating[13] which requires particular device geometries. Finding 2D materials with intrinsic robust ferromagnetism, including high T_c, large magnetic moment and reduced sample dimension remains an important challenge, as does the development of characterization tools, particularly related to electronic structure.

Here, we report robust 2D ferromagnetism in transition metal dichalcogenide, chromium ditelluride ($CrTe_2$) nanofilms. We show that it is possible to grow these films layer by layer on a graphene substrate. The electronic structure and magnetic properties are clearly resolved by angle-resolved photoemission spectroscopy (ARPES), superconducting quantum interference device (SQUID) and X-ray magnetic circular dichroism (XMCD). Bulk $CrTe_2$ single crystals are van der Waals (vdW) ferromagnets with T_c above room temperature (310 K)[14]. In this work, we successfully grow few-layer $CrTe_2$ films by the technique of molecular beam epitaxy (MBE). The robust ferromagnetism has been experimentally evidenced by both SQUID and XMCD

characterizations and persists up to 250 K (for a 7-monolayer (ML) $CrTe_2$ film of thickness 4.4 nm). In addition, the electron band structure of the ferromagnetic state was clearly resolved by *in-situ* ARPES. These results establish $CrTe_2$ nanofilms as an outstanding 2D ferromagnet.

The lattice structure of $CrTe_2$ is displayed in Fig. 1a, which shows the Cr and Te atoms forming a 1*T*-type sandwich layer. The $CrTe_2$ layers are stacked along the vertical direction. In our experiment, a bilayer graphene on SiC substrate was used to support a layer-by-layer growth of $CrTe_2$ films. The optical image of the samples is shown in the inset of Fig. 1b. The green areas are the surface of the SiC substrate while the grey area contains the epitaxial film. The MBE samples prepared this way can be of centimeter size with high structural uniformity. The microscopic topography taken from the surface of a 7 ML $CrTe_2$ film (Fig. 1b) shows atomically flat terrace. The step height between adjacent islands is 6.26 Å (Fig. 1e), which is consistent with the X-ray diffraction (XRD) characterization (Fig. 1d). The reflectivity curves show Laue fringes, indicating the high crystalline quality. The XRD was performed on a thick film of 39 layers, indicating that a large range of thickness from a few layers to tens of layers can be prepared by MBE. The atomic resolution images taken by *in-situ* scanning tunneling microscope (STM) on the same sample is presented in Fig. 1c, showing the hexagonal lattice structure. The lattice constant obtained from the line profile in Fig. 1f is 3.89 Å, in good agreement with the previous experimental results (3.79 Å)[14] and theoretical predictions (3.79 Å)[15].

The magnetic properties of the 7 ML $CrTe_2$ thin film were examined by SQUID measurements. Figure 2a shows a typical temperature-dependent magnetization (*M*-*T*), which clearly demonstrates a phase transition from paramagnetism to ferromagnetism as temperature decreases. The T_c increases from 253.6 K to 257.3 K as the field increases from 0.1 T to 0.5 T (Fig. S1). The field-dependent T_c reveals the 2D nature of the ferromagnetism, consistent with previous reports on magnetic control of transition temperatures in $Cr_2Ge_2Te_6$ thin flakes[2]. The in-plane and out-of-plane magnetization-magnetic field (*M*-*H*) loops at 20 K shown in Fig. 2b demonstrates a strong out-of-plane

anisotropy of the magnetization, also seen in other vdW ferromagnets[1,2,8]. This is an important consideration for obtaining ferromagnetic ordering and is also favorable for device applications. The *M-H* hysteresis loops plainly exhibit the ferromagnetic order in the 7 ML $CrTe_2$ film. Well-defined hysteresis loops were observed at elevated temperatures up to 250 K. At low temperature, a double-switching behavior is observed[16,17], which is possibly due to relatively weaker magnetic coupling between Cr magnetic moments at the interface. The temperature-dependent coercive field (H_c) derived from Fig. 2c confirms a strong ferromagnetism up to 250 K (Fig. 2d), consistent with *M-T* curve and further indicating the high T_c.

To further examine the out-of-plane magnetic ground state of 7 ML $CrTe_2$, element-specific XAS and XMCD measurements (Fig. 3a) were performed at the Cr $L_{2,3}$ edge. Typical XAS and XMCD spectra taken at 5 K with magnetic field of 1 T are plotted in Fig. 3b. Due to the octahedral coordination, the 3*d* orbitals of Cr^{3+} split into e_g and t_{2g} states with energy separation of 10 *Dq*. The t_{2g} states are filled with three unpaired electrons, while e_g states are empty. The XAS spectra of Cr present multiplet structures around photon energies of 575 eV and 584 eV, resulting from the excitations from Cr $2p_{3/2}$ and Cr $2p_{1/2}$ core levels, respectively. The small peak (~ 2 eV away from L_3 peak of Cr) marked with the black arrow comes from Te $5d_{5/2}$ core level, which slightly overlaps with the peak of Cr $2p_{3/2}$[18]. The fine structures at the higher energy side (marked with orange arrow) of the main features are related to the distribution of atomic multiplet. The observed structures are comparable with those measured from other Cr^{3+} compounds with octahedral coordination[19,20], providing a spectroscopic fingerprint of 1*T*-type $CrTe_2$. The measurements of XMCD and XAS were repeated at elevated temperatures, and the dichroism at Cr L_3 edge is evident up to 250 K. The characteristic peaks in the spectra remain at the same energy as the temperature rises, despite the decrease of intensity.

The XMCD results can be analyzed in terms of element-specific magnetic moments according to the sum rules[21,22]. The spin moment (m_s) and orbital moment (m_l) can be obtained by sum rule:

$$m_s = -n_h \frac{6\int_{L_3}(\sigma^- - \sigma^+)dE - 4\int_{L_{2,3}}(\sigma^- - \sigma^+)dE}{\int_{L_{2,3}}(\sigma^- + \sigma^+)dE} \times \mathrm{SC} - \langle T_z \rangle$$

$$m_l = -\frac{4}{3} n_h \frac{\int_{L_{2,3}}(\sigma^- - \sigma^+)dE}{\int_{L_{2,3}}(\sigma^- + \sigma^+)dE}$$

where n_h, SC and $\langle T_z \rangle$ are the number of d holes, spin correction factor (estimated to be 2.0 ± 0.2 for Cr)[9,23] and the averaged magnetic dipole term, respectively. The magnetic dipole term, $\langle T_z \rangle$ can be neglected due to its rather small contribution (<5%) in the Cr t_{2g}^3 configuration. An arctangent step-like function was employed in the fitting of the threshold of XAS spectra in order to exclude the nonmagnetic contribution[10,24].

The calculated m_s and m_l from 5-300 K are summarized in Fig. 3c. The derived m_s demonstrates a Curie-like behavior. A remarkably large value of m_s (2.85 ± 0.15 μ_B/atom) is found at 5 K. This reduces to 0.63 ± 0.15/atom at 250 K, suggesting a ferromagnetic transition near this temperature. By contrast, m_l is relatively flat and small (0.08 ± 0.05 μ_B/atom), consistent with a half-filled t_{2g} level. The octahedral crystal field (Fig. 1a) quenches m_l, because the three d electrons fully occupy the three-fold degenerate majority-spin t_{2g} orbital preventing orbital moment formation. The dichroism of Cr almost disappears when temperature increases to 300 K. Fitting the total magnetic moment ($m_t = m_s + m_l$) as a function of temperature, $\mathrm{M(T)} \propto \left(1 - \frac{T}{T_c}\right)^{\gamma}$, yields $T_c = 259 \pm 7$ K with critical exponent $\gamma = 0.48 \pm 0.08$, which is in good agreement with the SQUID result. We note that the observed ferromagnetic behavior cannot be due to Cr clusters, since Cr is antiferromagnetic and therefore would not give a non-zero XMCD intensity.

To examine the 2D electronic structure in $CrTe_2$ thin films, we performed ARPES measurements with two different photon energies of 21.2 eV and 40.8 eV at 107 K. The band dispersions measured at $h\nu$ = 21.2 eV along M-Γ-K is shown in Fig. 4a. Near the

Γ point, the main features include two hole-like valence bands, which are parallel aligned close to the Fermi level. Near the M point, there are two electron pockets with bottom locating at -1.2 eV and -1.8 eV, respectively. The well-resolved band structure indicates the high structural quality of the MBE-fabricated films. For a comparison, we calculated the spectrum of a 7 ML $CrTe_2$ slab by first-principles density functional method[25]. The mean free path of photoelectrons excited by photons of 21.2 eV and 40.8 eV is between 0.5 and 1 nm. Therefore, to compare with the experimental spectra, we simulated the band structure with a surface weight of each Bloch wavefunction. The higher intensity in the image means greater weight of wavefunction near the slab surface. Figure 4b shows the spin-polarized band structure, with the majority and minority spin bands plotted in red and blue, respectively. Both magnetization and spin orbit coupling (SOC) are taken into account in the calculation, and the magnetic moments are set along out-of-plane direction. The metallicity is a consequence of the hybridization of Te-*p* and Cr-*d* orbitals (Fig. S9) which leads to Te related bands crossing the Fermi level. The calculated majority band (left) and minority band (right) are separately plotted in Fig. 4c. The hole pockets near the Fermi level and the majority bands centered around Γ at binding energy E_B = 0.8 eV are mainly from the hybridization of Cr-3*d* and Te-5*p* orbitals (Fig. S9). There is an overall agreement between the experimental (Fig. 4a) and calculated band dispersions (Fig. 4b) except for the non-observation of two hole pockets from majority band near Γ point. We note that the two hole pockets near the Fermi level in Fig. 4d are mainly from the minority bands. By contrast, the majority hole pocket shows up in the spectrum taken at $h\nu$ = 40.8 eV (Fig. 4e) while the minority ones disappear. It suggests the emission from majority spin pockets was suppressed in our measurement at $h\nu$ = 21.2 eV as a consequence of matrix element effect[26]. The band dispersion can be traced by fitting the peak position in the momentum distribution curves (MDC), as marked by blue and red dashed lines in Fig. 4d and 4e, respectively. Combining the band structure near E_F taken by He Iα and He IIα photons together (Fig. 4f), the electronic structure is clearly metallic in both the majority and minority spin channels, and agrees well with DFT calculations. The

relatively small renormalizations needed to match with ARPES results suggest moderate-to-weak correlations. Furthermore, the experimental band structure of $CrTe_2$ is in sharp contrast with the band structure calculated without the inclusion of spin polarization (Fig. S7). The two hole pockets near E_F degenerate at Γ point in the calculated bands without spin polarization is similar to the experimental structure of monolayer VTe_2[27] and VSe_2[25,28]. The intrinsic spin-polarized electronic structure of the $CrTe_2$ film clearly demonstrates the magnetic phase of $CrTe_2$. In addition, the calculated magnetic moment on the Cr is 2.89 μ_B/atom, which is consistent with our SQUID and XMCD measurements.

Finally, we compare the magnetic properties of $CrTe_2$ films with other 2D magnets from literature[1,2,7,8,29-35] in Fig. 5. The T_c and magnetic moment per atom indicate the robustness and strength of ferromagnetism, respectively, both of which are important for applications. To date, the highest T_c of layered compounds is observed in bulk Fe_5GeTe_2 (310 K)[32]. The 7 ML $CrTe_2$ film has the highest T_c (259 K) among 2D materials in the quantum thickness regime. In addition, the $CrTe_2$ thin layers possess the largest magnetic moment per atom (~3 μ_B/atom), similar to that of CrI_3, $CrSiTe_3$ and $CrCl_3$. However, the T_c of CrI_3, $CrSiTe_3$ and $CrCl_3$ is much lower than room temperature. To collectively describe the robustness and strength of magnetic ordering, we plot the product of T_c and atomic magnetic moment for the known layered magnetic compounds in Fig. 5b. It shows clearly that the $CrTe_2$ epitaxial films possess extraordinary magnetic properties compared to other materials, and represent a highly promising platform for developing novel applications based on 2D magnetism.

In conclusion, robust ferromagnetism and large magnetic moment are observed in $CrTe_2$ thin films. The magnetization and strong dichroism can be observed up to 250 K. This work offers the first demonstration of XMCD and ARPES in 2D ferromagnetic epitaxial thin films, exhibiting an unambiguous evidence for the ferromagnetic ground state of Cr in $CrTe_2$ thin films. Unlike the exfoliated 2D magnets, which are typically of size less than 100 μm, the epitaxial magnetic films can readily reach wafer size with high structural quality. Therefore, the MBE growth of 2D ferromagnets based on $CrTe_2$

provides an ideal material platform for spintronics applications.

Methods

Growth of $CrTe_2$/bilayer graphene/SiC(0001) heterostructures. The 7 ML $CrTe_2$ thin film were grown on a bilayer graphene/SiC substrate in an integrated MBE-STM ultrahigh vacuum (UHV) system with base pressure below 2×10^{-10} mbar. The bilayer graphene was prepared by annealing a 6H SiC(0001) substrate at 1150 °C for 20 seconds and repeating 30 times. Then, high-purity Cr and Te were evaporated from an electron-beam evaporator and a standard Knudsen cell, respectively, with a flux ratio of 1:10. The temperature of substrate was kept at 375 °C during the growth. The deposition rate of Cr and Te atoms was monitored by a quartz oscillator. In order to protect the thin film from contamination and oxidation during SQUID and XMCD measurements, a Te capping layer (~5 nm) was deposited on sample surface after growth.

Magnetization characterizations. The magnetization measurements were performed by using a Quantum Design superconducting quantum interference device (SQUID) magnetometer with magnetic field up to 7 T.

X-ray absorption spectroscopy and X-ray magnetic circular dichroism. The experiments were performed on beamline I10 at Diamond Light Source, U.K., with 100% circularly polarized X-ray perpendicular to the sample plane and parallel to the magnetic field. XAS measurements with total electron yield (TEY) mode were carried out from 5 K to 300 K. By flipping the X-ray helicity at fixed magnetic field of 1 T, we obtained XMCD by taking the difference of XAS, σ^{-}- σ^{+}.

X-ray diffraction. High-resolution x-ray diffraction was performed using $MoK_{\alpha1}$ radiation (0.70926 Å) which was obtained from a flat perfect crystal Ge monochromator that produced a line beam having angular divergence of in the scattering plane and out of the scattering plane. The measurements were performed by specular reflection

and the data were modeled using the reflection amplitudes from the substrate, several graphene layers, layers of $CrTe_2$ and its structure factor[32].

Angle-resolved photoemission spectroscopy and scanning tunneling microscopy. After the growth, the film was transferred *in-situ* to the ARPES stage. ARPES measurements were performed at 107 K using a SPECS PHOIBOS 150 hemisphere analyzer with a SPECS UVS 300 helium discharge lamp (He Iα = 21.2 eV and He IIα = 40.8 eV). The energy resolution is 40 meV under 107 K. The topography of the sample surface was mapped *in-situ* by an Aarhus STM.

First-principles calculations. We have performed first-principles calculations with density functional theory as implemented in the VASP package. We used the Perdew-Burke-Ernzerhof (PBE) form for the exchange-correlation functional with a plane-wave cut-off energy of 300 eV. The super cell includes seven $CrTe_2$ layers and a vacuum layer of about 20 Å. The $CrTe_2$ layers are allowed to relax during the geometry optimization.

Acknowledgments

This work is supported by the National Key Research and Development Program of China (No. 2016YFA0300803, No. 2017YFA0206304), the National Basic Research Program of China (No. 2014CB921101), the National Natural Science Foundation of China (No. 61427812, 11774160, 11574137, 61474061, 61674079), Jiangsu Shuangchuang Program, the Natural Science Foundation of Jiangsu Province of China (No. BK20140054), UK EPSRC (EP/S010246/1), leverhulme Trust (LTSRF1819\15\12), and Royal Society (IEC\NSFC\181680). Diamond Light Source is acknowledged to I10 under proposal MM22532. G.B. is supported by the US National Science Foundation (NSF-DMR#1809160). T.-R.C. is supported by the Young Scholar Fellowship Program from the Ministry of Science and Technology (MOST) in Taiwan, under a MOST grant for the Columbus Program MOST108-2636- M-006-002,

National Cheng Kung University, Taiwan, and National Center for Theoretical Sciences, Taiwan. This work is also partially supported by the MOST, Taiwan, Grant MOST107-2627-E-006-001 and by Higher Education Sprout Project, Ministry of Education to the Headquarters of University Advancement at National Cheng Kung University (NCKU).

Author contributions

G.B.,Y.X. and L.H planned the project. X.Z. and Q.L. synthesized $CrTe_2$ thin films. Q.L., X.Z. and J.C. conducted the ARPES and STM experiments and analyzed the data. W.L., J.S. and W.N. performed XMCD and SQUID measurements and analyzed the data. Q.L., S.-W.L., T.-R.C. and D.J.S did the DFT calculations. P.M. and M.V. conducted XRD measurements. X.Z., Q.L., D.J.S and G.B. wrote the paper. All the authors discussed the results and commented on the manuscript.

Competing financial interests

The authors declare no competing financial interests.

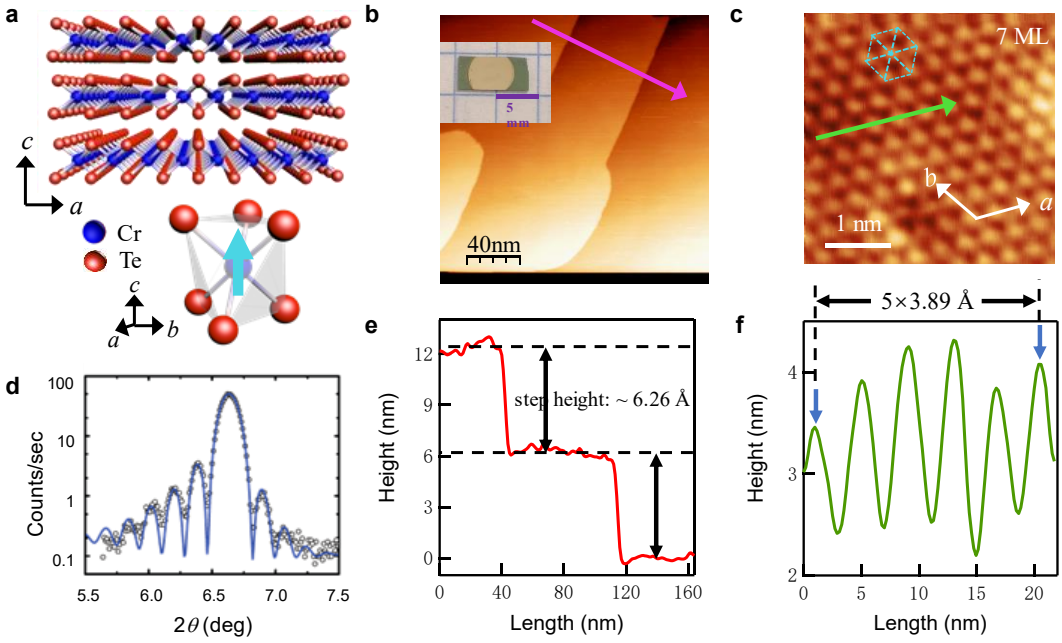

Figure 1. Crystal structure and STM characterization of epitaxially grown $CrTe_2$ thin films. **a**, Side view of the crystal structure of $CrTe_2$ with a light blue arrow representing the out-of-plane magnetic moment. **b**, The STM topography image (200 × 200 nm^2) of 7 ML $CrTe_2$ fabricated on graphene/SiC. U = +1 V, I_t = 200 pA. The inset shows the optical image of the sample. **c**, Atom-resolved STM image (4 × 4 nm^2) of 7 ML $CrTe_2$ with hexagonal structure (light blue dotted lines). U = -1.5 mV, I_t = -440 pA. **d**, X-ray diffraction shows Laue fringes around the (001) $CrTe_2$ reflections, indicating a highly uniform film. The solid curve is a fit to a model that contains 39 layers of $CrTe_2$ and 2 unit cells of roughness with a lattice constant c = 6.13 Å. **e**, The line-scan profile taken along the pink arrowed line in **b**, with an average step height of ~ 6.26 Å. **f**, The line-scan along the green arrow from **d** showing an atomic periodicity of ~3.89 Å.

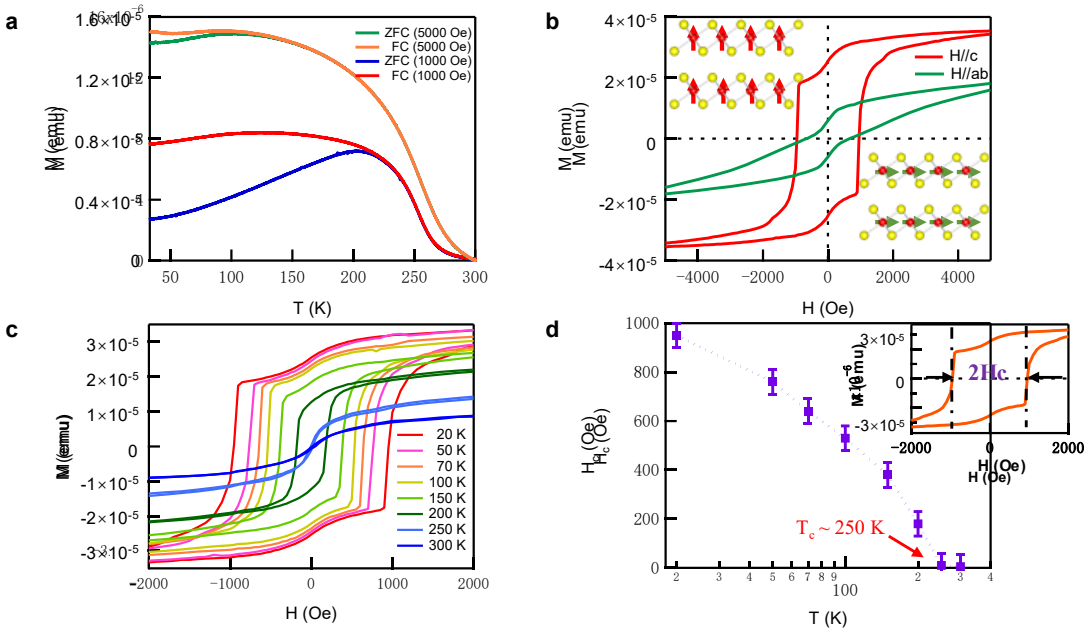

Figure 2. SQUID measurements of ferromagnetic $CrTe_2$ thin films with out-of-plane anisotropy. **a**, Zero-field and field cooled temperature dependence of the magnetization of 7 ML $CrTe_2$ with an applied in-plane magnetic field of 0.1 T and 0.5 T. **b**, Magnetic hysteresis loops at 20 K with external field in both the perpendicular and parallel orientation with respect to sample plane, showing a ferromagnetic behavior. The easy axis is determined to be out-of-plane. **c**, Enlarged view of the temperature-dependent out-of-plane magnetic moment. **d**, The H_c versus temperature of $CrTe_2$ derived from **c**, displaying a decreased value of H_c as temperature increases. Inset: the definition of H_c from a magnetic hysteresis loop.

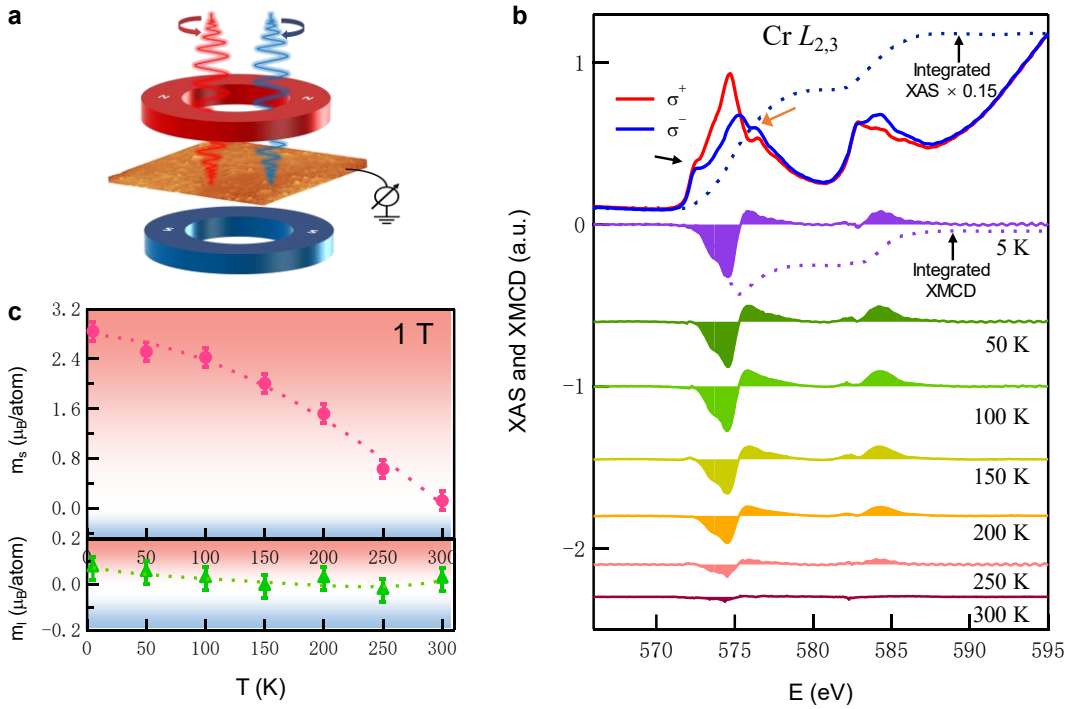

Figure 3. XAS and XMCD characterizations of 7 ML $CrTe_2$ thin film. a, Schematic geometry of XMCD experimental setup. **b**, XAS and XMCD spectra of $CrTe_2$ from 5 K to 300 K (spectra at different temperatures are offset for clarity). **c**, m_s *and* m_l versus temperature derived from **a** using sum rules with the fitting lines, which exhibits a Curie-like behavior with $T_c \sim 259 \pm 7$ K.

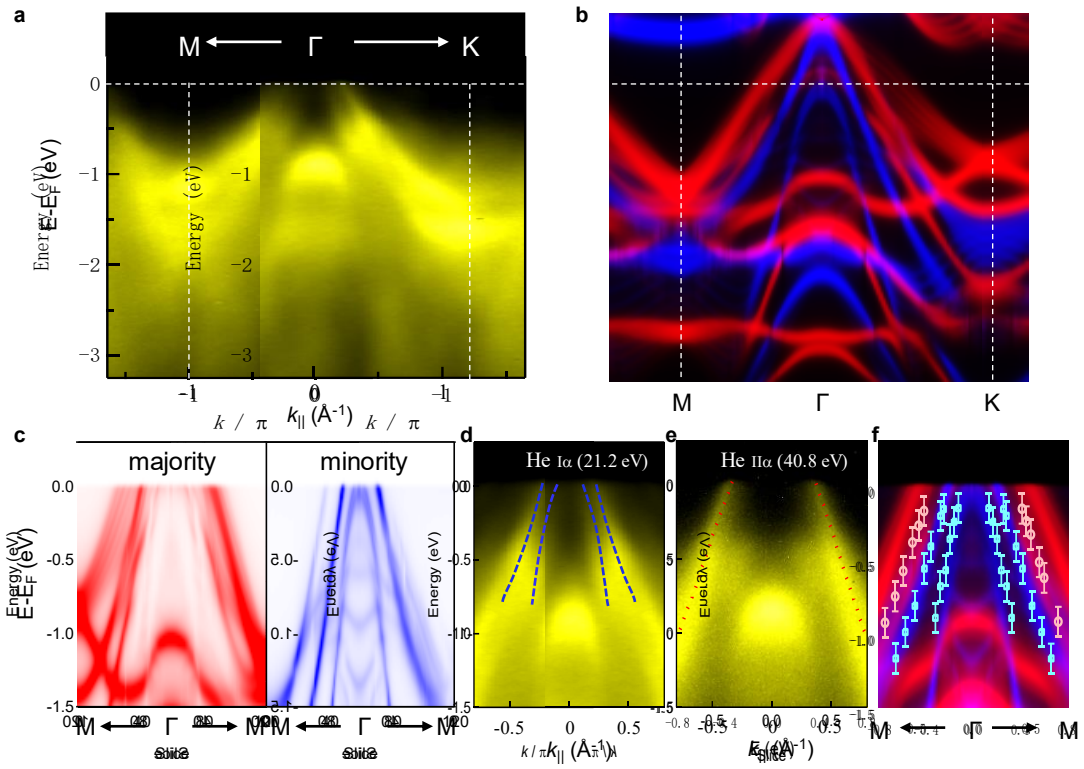

Figure 4. ARPES band mapping of 7 ML $CrTe_2$ thin film compared to first-principles results. a,b, Plots of APRES spectrum (a) and the first-principles bands (b) along M-Γ-K with the inclusion of spin polarization. The majority and minority spin bands are plotted in red and blue colors, respectively. **c,** The calculated majority (left) and minority bands (right). **d-f,** Comparison of the valence-band dispersion near the Fermi level taken with He Ia (21.2 eV) (d), He IIa photons (40.8 eV) (e) with theoretical bands (f) along the high symmetry direction M-Γ-M. The blue and red dashed lines indicate the position of hole pockets measured by He Ia and He IIa photons, respectively. The light blue/red markers with error bars represent the position of MDC peaks.

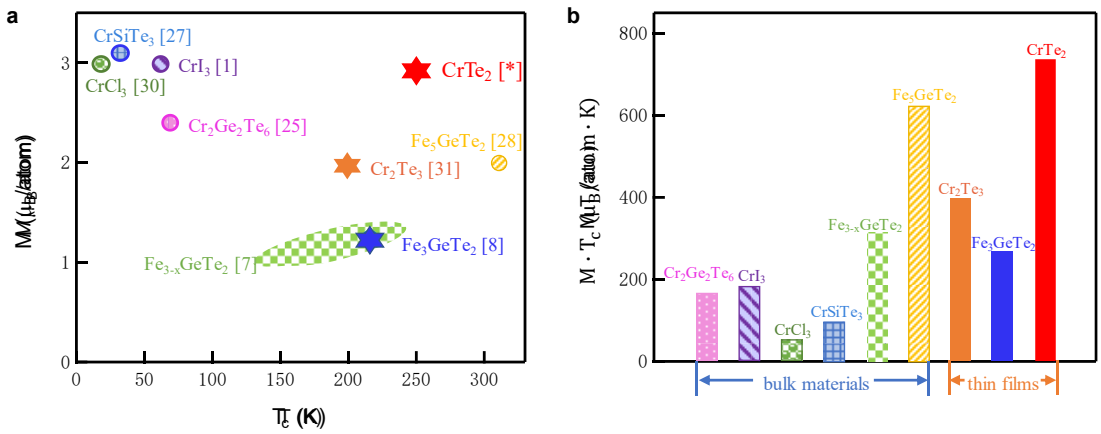

Figure 5. Intrinsic T_c and saturated magnetic moment of the $CrTe_2$ thin film and other known 2D magnets. a, The experimental values of intrinsic T_c and saturated magnetic moment of the 7 ML $CrTe_2$ [*] and various 2D magnets at low temperatures ($T \ll T_c$). The stars represent MBE-grown thin films, while circles and ellipses indicate bulk materials or exfoliated flakes. **b**, A combined parameter, $M \cdot T_c$, describing the robustness and strength of magnetic ordering, is presented in the histogram.

Table 1. Intrinsic T_c of 2D Magnets from previous works[a]

Materials	T_c (K)	M (m_B/atom)	ref
7 ML $CrTe_2$ thin film	254	2.93	[*]
10 ML Fe_3GeTe_2 thin film	216	1.23	8
Cr_2Te_3 thin film	170	1	35
Bilayer $Cr_2Ge_2Te_6$ flake	28		2
1 ML CrI_3 flake	45		1
$CrSiTe_3$ bulk	31	3.1	31
$CrCl_3$ bulk	17	3	34
$Cr_2Ge_2Te_6$ bulk	68	2.4	29
Fe_5GeTe_2 bulk	310	2	32
$Fe_{3-x}GeTe_2$ bulk	140 ~ 232	1.04 ~ 1.32	7
CrI_3 bulk	61	3	1

[a] Typical values of T_c from previous reports. Our work [*] demonstrates a large T_c and magnetic moment among them.

Reference

1 Huang, B. *et al.* Layer-dependent ferromagnetism in a van der Waals crystal down to the monolayer limit. *Nature* **546**, 270-273 (2017).

2 Gong, C. *et al.* Discovery of intrinsic ferromagnetism in two-dimensional van der Waals crystals. *Nature* **546**, 265-269 (2017).

3 Song, T. *et al.* Giant tunneling magnetoresistance in spin-filter van der Waals heterostructures. *Science* **360**, 1214–1218 (2018).

4 Ding Zhong & Seyler, K. L. Van der Waals engineering of ferromagnetic semiconductor heterostructures for spin and valleytronics. *Sci. Adv.* **3**, e1603113 (2017).

5 Seyler, K. L. *et al.* Ligand-field helical luminescence in a 2D ferromagnetic insulator. *Nat. Phys.* **14**, 277-281 (2017).

6 Wang, Z. *et al.* Electric-field control of magnetism in a few-layered van der Waals ferromagnetic semiconductor. *Nat. Nanotechnol.* **13**, 554-559 (2018).

7 May, A. F., Calder, S., Cantoni, C., Cao, H. & McGuire, M. A. Magnetic structure and phase stability of the van der Waals bonded ferromagnet $Fe_{3-x}GeTe_2$. *Phys. Rev. B* **93**, 014411 (2016).

8 Liu, S. *et al.* Wafer-scale two-dimensional ferromagnetic Fe_3GeTe_2 thin films grown by molecular beam epitaxy. *Npj 2D Mater. Appl.* **1**, 30 (2017).

9 Liu, W. *et al.* Enhancing magnetic ordering in Cr-doped Bi_2Se_3 using high-T_C ferrimagnetic insulator. *Nano Lett.* **15**, 764-769 (2015).

10 Liu, W. Q. *et al.* Atomic-Scale Interfacial Magnetism in Fe/Graphene Heterojunction. *Sci. Rep.* **5**, 11911 (2015).

11 He, Q. L. *et al.* Exchange-biasing topological charges by antiferromagnetism. *Nat. Commun.* **9**, 2767 (2018).

12 Tang, C., Chang, C.-Z., Zhao, G. & Liu, Y. Above 400-K robust perpendicular ferromagnetic phase in a topological insulator. *Sci. Adv.* **3**, e1700307 (2017).

13 Deng, Y. *et al.* Gate-tunable room-temperature ferromagnetism in two-dimensional Fe_3GeTe_2. *Nature* **563**, 94-99 (2018).

14 Freitas, D. C. Ferromagnetism in layered metastable 1*T*-$CrTe_2$. *J. Phys.: Condens. Matter* **27**, 176002 (2015).

15 Lv, H. Y. Strain-controlled switch between ferromagnetism and antiferromagnetism in 1T-CrX_2 (X = Se, Te) monolayers. *Phys. Rev. B* **92**, 214419 (2015).

16 Olejnik, K. *et al.* Exchange bias in a ferromagnetic semiconductor induced by a ferromagnetic metal: Fe/(Ga,Mn)As bilayer films studied by XMCD measurements and SQUID magnetometry. *Phys. Rev. B* **81**, 104402, doi:10.1103/PhysRevB.81.104402 (2010).

17 He, Q. L. *et al.* Tailoring exchange couplings in magnetic topological-insulator/antiferromagnet heterostructures. *Nat. Mater.* **16**, 94-100 (2017).

18 Ye, M. *et al.* Carrier-mediated ferromagnetism in the magnetic topological insulator Cr-doped $(Sb,Bi)_2Te_3$. *Nat. Commun.* **6**, 8913 (2015).

19 Ishida, Y. *et al.* X-ray Magnetic Circular Dichroism and Photoemission Study of the Diluted Ferromagnetic Semiconductor $Zn_{1-x}Cr_xTe$. *Appl. Phys. Express* **1**, 041301 (2008).

20 Kobayashi, M. *et al.* Local electronic structure of Cr in the II–VI diluted ferromagnetic semiconductor $Zn_{1-x}Cr_xTe$. *New J. Phys.* **10**, 055011 (2008).
21 Chen, C. T. *et al.* Experimental confirmation of the X-ray magnetic circular dichroism sum rules for iron and cobalt. *Phys. Rev. Lett.* **75**, 152-155 (1995).
22 van der Laan, G. & Thole, B. T. Strong magnetic x-ray dichroism in 2*p* absorption spectra of 3dtransition-metal ions. *Phys. Rev. B* **43**, 13401-13411 (1991).
23 Liu, W. *et al.* Atomic-Scale Magnetism of Cr-Doped Bi_2Se_3 Thin Film Topological Insulators. *ACS nano* **9**, 10237-10243 (2015).
24 Liu, W. *et al.* Experimental Observation of Dual Magnetic States in Topological Insulators. *Sci. Adv.* **5**, eaav2088 (2019).
25 Wong, P. K. J. *et al.* Evidence of Spin Frustration in a Vanadium Diselenide Monolayer Magnet. *Adv. Mater.*, e1901185 (2019).
26 Belopolski, I. *et al.* Discovery of topological Weyl fermion lines and drumhead surface states in a room temperature magnet. *Science* **365**, 1278 (2017).
27 Wang, Y., Ren, J. & Li, J. Evidence of charge density wave with anisotropic gap in monolayer VTe_2 film. *arXiv* **1905**, 13446 (2019).
28 Feng, J. *et al.* Electronic Structure and Enhanced Charge-Density Wave Order of Monolayer VSe_2. *Nano Lett.* **18**, 4493-4499 (2018).
29 Xing, W. *et al.* Electric field effect in multilayer $Cr_2Ge_2Te_6$: a ferromagnetic 2D material. *2D Mater.* **4**, 024009 (2017).
30 Zhang, X. *et al.* Magnetic anisotropy of the single-crystalline ferromagnetic insulator $Cr_2Ge_2Te_6$. *Jpn. J. Appl. Phys.* **55**, 033001 (2016).
31 Liu, B. J. *et al.* Critical behavior of the quasi-two-dimensional semiconducting ferromagnet $CrSiTe_3$. *Sci. Rep.* **6**, 33873 (2016).
32 May, A. F. *et al.* Ferromagnetism Near Room Temperature in the Cleavable van der Waals Crystal Fe_5GeTe_2. *ACS nano* **13**, 4436-4442 (2019).
33 Mogi, M. *et al.* Ferromagnetic insulator $Cr_2Ge_2Te_6$ thin films with perpendicular remanence. *APL Mater.* **6**, 091104 (2018).
34 McGuire, M. A. *et al.* Magnetic behavior and spin-lattice coupling in cleavable van der Waals layered $CrCl_3$ crystals. *Phys. Rev. Mater.* **1**, 014001 (2017).
35 Chen, J. *et al.* Evidence for Magnetic Skyrmions at the Interface of Ferromagnet/Topological-Insulator Heterostructures. *Nano Lett.* **19**, 6144 (2019).